Historical Shifts in Seasonality and Timing of Extreme Precipitation

Gründemann, G. J.; Zorzetto, E.; van de Giesen, N.; van der Ent, R. J.

Important note
To cite this publication, please use the final published version (if applicable).
Please check the document version above.

AGU ADVANCING EARTH AND SPACE SCIENCES

Geophysical Research Letters®

Author Contributions:

Conceptualization: G. J. Gründemann, E. Zorzetto, R. J. van der Ent
Data curation: G. J. Gründemann
Formal analysis: G. J. Gründemann
Methodology: G. J. Gründemann, E. Zorzetto, R. J. van der Ent
Project Administration: G. J. Gründemann
Software: G. J. Gründemann, E. Zorzetto
Supervision: R. J. van der Ent
Validation: G. J. Gründemann
Visualization: G. J. Gründemann, N. van de Giesen
Writing – original draft: G. J. Gründemann
Writing – review & editing: G. J. Gründemann, E. Zorzetto, N. van de Giesen, R. J. van der Ent

Historical Shifts in Seasonality and Timing of Extreme Precipitation

G. J. Gründemann[1,2] , **E. Zorzetto[3]**, **N. van de Giesen[1]** , and **R. J. van der Ent[1]**

[1]Department of Water Management, Faculty of Civil Engineering and Geosciences, Delft University of Technology, Delft, The Netherlands, [2]Centre for Hydrology, University of Saskatchewan, Canmore, AB, Canada, [3]Program in Atmospheric and Oceanic Sciences, Princeton University, Princeton, NJ, USA

Abstract Global warming impacts the hydrological cycle, affecting the seasonality and timing of extreme precipitation. Understanding historical changes in extreme precipitation occurrence is crucial for assessing their impacts. This study uses relative entropy to analyze historical changes in seasonality and timing of extreme daily precipitation occurrences on the global domain for 63 years of fifth generation of the European Reanalysis reanalysis data. Our analysis reveals distinct regional patterns of change. During the second half of the 20th century, Africa and Asia experienced high clustering of precipitation extremes. Over the past 60 years, clustering increased in Africa while becoming more spread out in Asia. North America and Australia had initially lower clustering and showed slight increases over time. Extreme events in extra-tropical land regions mainly occurred in summer, with modest shifts in timing. These findings have implications for risk assessments of natural hazard like flash floods and landslides, emphasizing the necessity for region-specific adaptation strategies.

Plain Language Summary Global warming is changing how and when heavy rain and extreme weather events happen. It is important to understand these changes for planning and preparing for floods and other water-related problems. In this study, we looked at long records of rainstorms to see how they have changed over time. We found that different regions have experienced different changes. During the second half of the 20th century, Africa and Asia were regions with the strongest seasonality. Over the 60 years we analyzed, seasonal clustering overall increased in Africa, while in Asia they became more spread out throughout the year. In Europe, North America and Australia, rainstorms were more spread out throughout the year but became slightly more concentrated. Most of the heavy rainstorms outside the tropics happened in summer, with a small shift in timing. These findings show how various regions have experienced different changes, which is important to take into account when planning and preparing for floods.

1. Introduction

Global warming is known to intensify the water cycle, leading to an increase in climate extremes (Allen & Ingram, 2002; Easterling et al., 2016; IPCC, 2012). Historical data reveals increases in observed precipitation extremes (Alexander, 2016; Asadieh & Krakauer, 2015; Papalexiou & Montanari, 2019), and projections indicate further intensification in the future (e.g., Donat et al., 2016; Fowler et al., 2021; Gründemann et al., 2022; Meredith et al., 2019; Moustakis et al., 2021; Pendergrass & Knutti, 2018; Pfahl et al., 2017; Tandon et al., 2018; Westra et al., 2014). Yet, these patterns and shifts are not uniform across the world. Factors such as topography, oceanic cycles and atmospheric patterns influence the spatiotemporal distribution and seasonality of extreme precipitation events (Dey et al., 2021; Fernandes & Rodrigues, 2018; Gründemann et al., 2023a; Haylock et al., 2006). In tropical regions for instance, extreme precipitation predominantly occurs during monsoon seasons, with monsoon-affected areas witnessing an expansion, intensification of rains, and a prolonged monsoon season (Chen & Sun, 2013; Kitoh et al., 2013). In contrast, mid-latitudes often experience precipitation extremes during the transitional seasons, with many Mediterranean basins observing a shift to earlier in the year (Tramblay et al., 2023). Polar regions, meanwhile, are witnessing an increase in precipitation extremes during summer, with a transition from snow to more rain (Landrum & Holland, 2020; Loeb et al., 2022; Wang et al., 2021).

Changes in seasonality of extreme precipitation can have negative impacts on hydrological systems, agriculture, and overall water resource management (Kundzewicz et al., 2018). Additionally, shifts in precipitation seasonality affects flood patterns (Berghuijs et al., 2019; Blöschl et al., 2017; Wasko et al., 2020a, 2020b) and the

occurrence of natural hazards, such as flash floods, landslides (Marc et al., 2018; Steger et al., 2023), and debris flow (Nikolopoulos et al., 2015). Moreover, these changes interact with other climate feedback mechanisms, such as snowmelt runoff, atmospheric rivers, and tropical cyclones, amplifying or mitigating the impacts of climate change on various parts of the hydrological cycle (Gershunov et al., 2017; Miniussi et al., 2020; Tarasova et al., 2023).

In recent decades, relative entropy has emerged as a valuable tool to study the seasonality of precipitation and its extremes. Rooted in statistical physics and information theory (Cover & Thomas, 2005; Greven et al., 2014), this method quantifies the statistical distance between the actual distribution of extreme precipitation occurrences and a uniform distribution (Kullback & Leibler, 1951). Feng et al. (2013) introduced this tool to the field of precipitation research to study the seasonality of monthly rainfall in tropical regions. Since, several studies have used relative entropy to study rainfall seasonality across different time scales and geographical regions (Bal et al., 2019; Limsakul, 2020; Moustakis et al., 2021; Pascale et al., 2015, 2016; Sahany et al., 2018). Hitherto, however, a comprehensive global scale assessment of historically observed changes in timing and seasonality of extreme precipitation is missing.

This study aims to bridge this gap by evaluating the seasonality and timing of extreme daily precipitation. Using the relative entropy measure, we assess the degree of seasonality in extreme precipitation and to evaluate historical trends. By defining extreme precipitation above a relative threshold, we investigate the spatial patterns of these changes across different regions. We use the fifth generation of the European Reanalysis (ERA5) reanalysis data set, which provides high-quality and relatively homogeneous precipitation data, allowing for a comprehensive analysis of the observed changes in extreme precipitation seasonality.

2. Materials and Methods

2.1. Data

Precipitation data were obtained from the ERA5 reanalysis data set (Hersbach et al., 2018, 2020). This data set was chosen for its continuous coverage and relatively long temporal span at high spatial and temporal resolutions. While reanalysis data sets provide a comprehensive estimate of the global atmosphere-land-ocean system, it has known issues in accurately simulating convective processes, data assimilation inconsistencies, and limited observations over areas like oceans. The performance of ERA5 in capturing precipitation extremes varies depending on the intensity and location (Lei et al., 2022). ERA5 performs well over the extra-tropics, but exhibits larger errors over the tropics (Lavers et al., 2022). Notably, while ERA5 tends to underestimate the heaviest precipitation events, it reliably captures their general patterns, locations, and magnitude of less intense events (Bandhauer et al., 2022; Hénin et al., 2018; Lavers et al., 2022; Shen et al., 2022).

Hourly precipitation data from 01-01-1959 to 31-12-2021 at a resolution of 0.25° latitude × 0.25° longitude (approximately 30 by 30 km at the equator). These data were aggregated into daily estimates covering 63 years. The analysis involved moving 30-year windows through the data set, starting with the first 30 years (01-01-1959 to 31-12-1988) and shifting forward by one calendar year for each new 30-year segment. This resulted in 33 such 30-year windows.

2.2. Precipitation Extremes

We defined precipitation extremes as the highest 3 events per year on average, corresponding to the highest 90 events per 30-year window (or the 99.18th percentile of all day precipitation, or a return period of 0.335 years). Different thresholds were explored to quantify rainfall extremes across various regions, with little impact on the observed trends. Inclusion of more events reduced seasonality (see Figure S1 in Supporting Information S1), likely because that incorporates precipitation from various precipitation-generating mechanisms which may be characterized by different magnitudes and seasonal occurrence. This results in more evenly distributed occurrences throughout the year.

2.3. Relative Entropy as a Measure for Seasonality

To assess the seasonality of extreme precipitation occurrences, we use Relative Entropy, also known as Kullback-Leiber distance (D_{KL}; Kullback & Leibler, 1951). Relative entropy is a measure of the statistical distance
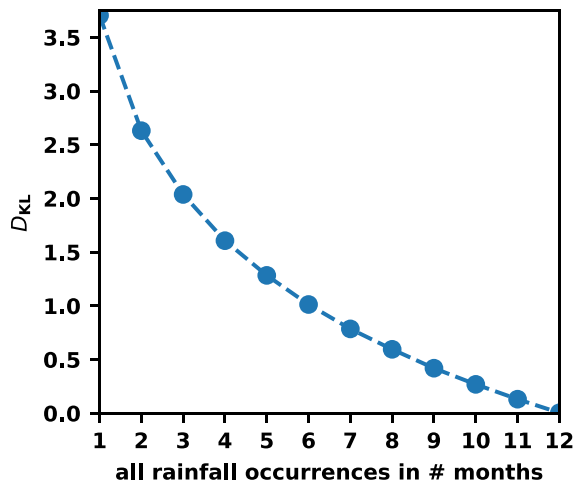
Figure 1. The value of the relative entropy D_{KL} (Equation 1) when all extreme rainfall occurrences are evenly distributed over 1–12 months.

between two probability distributions: (a) the actual monthly distribution of extreme precipitation occurrences and (b) the uniform distribution (Cover & Thomas, 2005). The calculation of relative entropy (D_{KL}) is represented by the following equation:

$$D_{KL} = \sum_{m=1}^{12} p_m \log_2\left(\frac{p_m}{q_m}\right) \tag{1}$$

In this equation, p_m represents the actual probability distribution of monthly extreme precipitation occurrences, while q_m denotes the uniform distribution of monthly occurrences. p_m is calculated by dividing the number of monthly extreme precipitation occurrences (n_m) by the total number of occurrences ($N = 90$). Therefore, $p_m = n_m/N$. The uniform distribution (q_m) is approximately 0.083 for each month, taking into account the actual number of days in each month. The resulting value of D_{KL} is measured in bits, as the base of the logarithm is 2 (Cover & Thomas, 2005), with a range between 0.005 and 3.7. Higher values indicate a clustering of extreme precipitation occurrences, while lower values suggest a more evenly spread distribution throughout the year. Figure 1 serves as a reference to aid in the interpretation of D_{KL}. A single D_{KL} value is calculated for each 30-year window, resulting in 33 values per grid cell. We note that if two areas have a similar D_{KL} value, that does not mean that the rainfall events in both areas have similar magnitude, precipitation-generating mechanism, or timing.

2.4. Timing

To evaluate the timing and duration of precipitation extremes, the centroid (C) and the spread (Z) of the seasonal distribution were computed as the first and second moments of n_m, respectively. The formulas for calculating C and Z are as follows:

$$C = \frac{1}{N} \sum_{m=1}^{12} m \times n_m \tag{2}$$

$$Z = \sqrt{\frac{1}{N} \sum_{m=1}^{12} |m - C|^2 \times n_m} \tag{3}$$

C represents the timing, while Z indicates clustering of the extremes around the centroid. Even though C can be estimated for each grid cell, it is not useful for locations with low D_{KL} values, as there is no clear clustering of extremes. These metrics were only estimated for gridcells where the mean $D_{KL} > 0.27$, indicating clustering of extremes in less than 10 months. To address potential errors related to events around November to February, a 6-month shift was applied and C and Z were recalculated and then shifted 6 months back, yielding C_{shift} and Z_{shift}. The choice between the original and shifted values depended on which produced a lower mean spread for each grid cell. The mean of the original C and C_{shift} as well as Z and Z_{shift} are included in Figure S2 in Supporting Information S1. Another approach to do this is using the circular mean as in Dey et al. (2021), but it yields similar results.

2.5. Regional Analysis

The regional analysis was conducted for IPCC WGI reference regions (WGI-v4; Iturbide et al., 2020), focusing on land regions. We pooled all events within a region, weighed them by cell size, and calculated the regional D_{KL}, C and Z (Equations 1–3). To ensure a focus on regions with significant precipitation patterns, areas with very low rainfall, such as the Sahara, were excluded from this study. These dry areas were identified as cells where the mean value of the 90th highest rainfall event in the 30-year windows was below 5 mm day^{-1} (gray cells in Figure 2a). In the regional analysis, we only included regions containing at least 50% of the cells meeting this criterion, excluding the Sahara, Arabian Peninsula, and Eastern Antarctica.
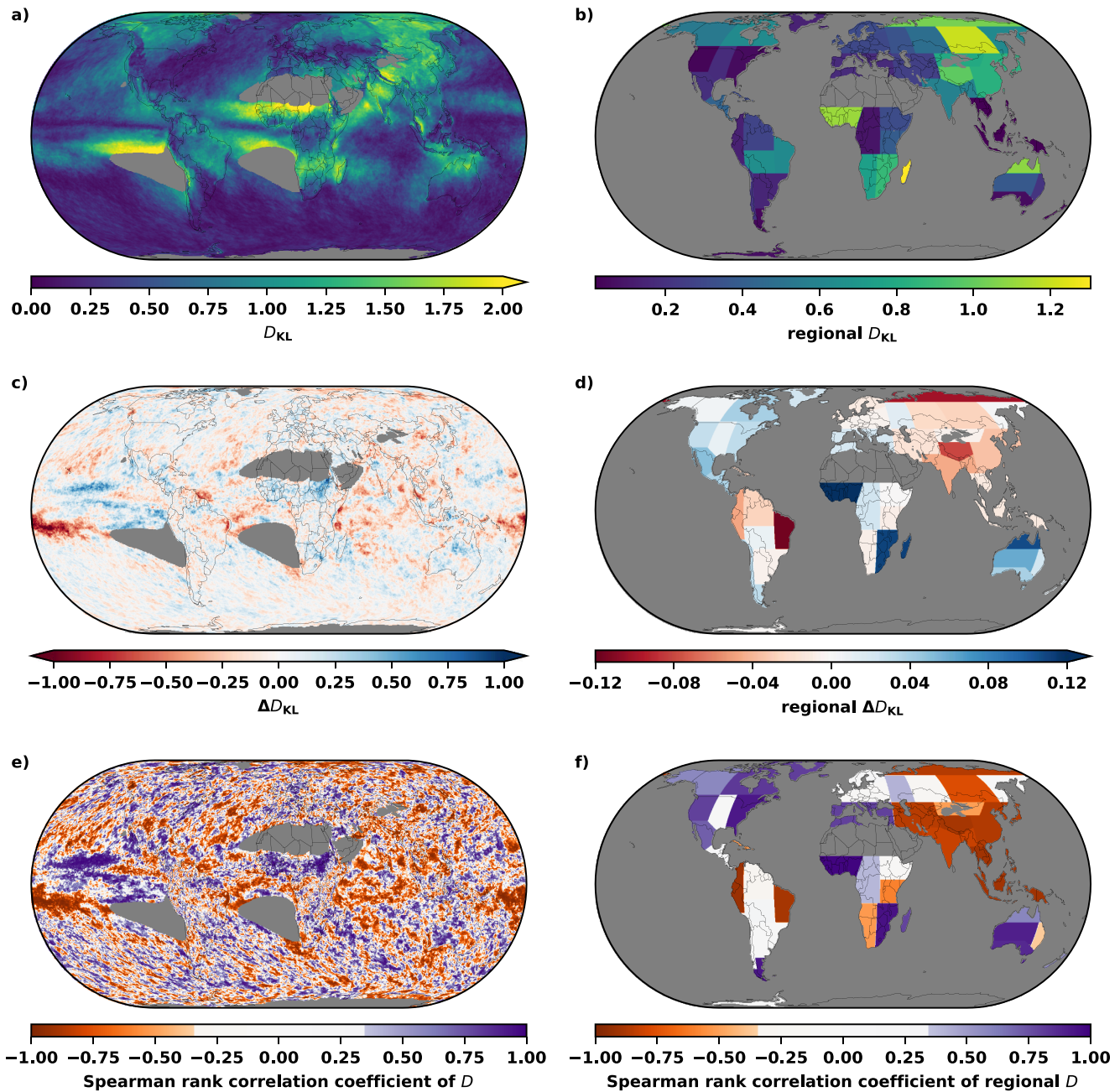
Figure 2. Relative entropy of extreme daily precipitation occurrences (D_{KL}, Equation 1). Presented as (a) the mean of all 30-year windows analyzed per grid cell, where a low value signifies an even distribution of extreme rainfall throughout the year, and a high value suggest clustering in a specific period. Panel (b) shows D_{KL} calculated per WGI-v4 reference region over land. Panel (c) shows the difference in D_{KL} between the first land last windows for each grid cell ($\Delta D = D_{1992-2021} - D_{1959-1988}$), with a negative ΔD indicating a more even distribution of rainfall extremes and a positive ΔD indicating more clustering. Panel (d) shows the same difference calculated per WGI-v4 reference region over land. Panel (e) shows the Spearman rank correlation coefficient of D_{KL} over time, the non-white values indicate statistical significance ($p < 0.05$). Panel (f) shows the correlation coefficients calculated per WGI-v4 reference region over land. Dry areas, defined as cells with a mean value of the 90th highest rainfall event in all 30-year windows below 5 mm day^{-1}, are masked in gray. Regions in panels (b), (d) and (f) only include those containing at least 50% of the cells.

2.6. Statistical Significance

Spearman rank correlation was performed to assess positive and negative monotonic relationships between D_{KL} and C over time in grid cells and regions. The correlation coefficient (ρ) ranges from -1 to 1, indicating the strength of the relationship. Significance was determined for $p < 0.05$. We also have repeated this analysis testing

Table 1
Statistical Significance (p < 0.05) of D_{KL} Trends With Time, Using the Spearman Rank Correlation Coefficient

	Global	Global land
Correlation coefficient significant	73.0%	73.4%
- of which positively	47.9%	50.1%
- of which negatively	52.1%	49.9%

Note. Dry areas, namely the cells in which the mean value of the 90th highest rainfall event in the 30-year windows is below 5 mm day^{-1}, are not included.

for field significance, following the false discovery rate approach described in Wilks (2016, Equation 3), with minimal impact detected (see Figure S3 in Supporting Information S1).

3. Results

Figure 2a displays the relative entropy (D_{KL}) of daily extreme precipitation occurrences as the mean value over all 30-year windows per grid cell. D_{KL} follows geographical features like mountain ranges and coastlines. Notably, mountain peaks exhibit low D_{KL} values, while slopes have higher values. Examples are found in the Andes, Patagonia, Scandinavia, Ural Mountains, and Himalayas. Coastlines also display distinctive D_{KL} patterns, with land areas often exhibiting higher values compared to adjacent oceans, seen around western Europe and Morocco, the Red Sea, the coast of eastern Africa, eastern Madagascar, western India, Myanmar, eastern Malaysia, and western Australia. In ERA5, D_{KL} is generally higher on land than over oceans, with the exceptions of the South Pacific ocean, subtropical Atlantic and Arabian Sea. Panel b shows the D_{KL} for each WGI-v4 reference region over land, with regions like Madagascar, Western Africa, and parts of Asia displaying the highest regional D_{KL} values. Conversely, Eastern and Western United States, Southern South America, Southeast Asia and Southern Australia and New Zealand exhibit the lowest D_{KL} values on land.
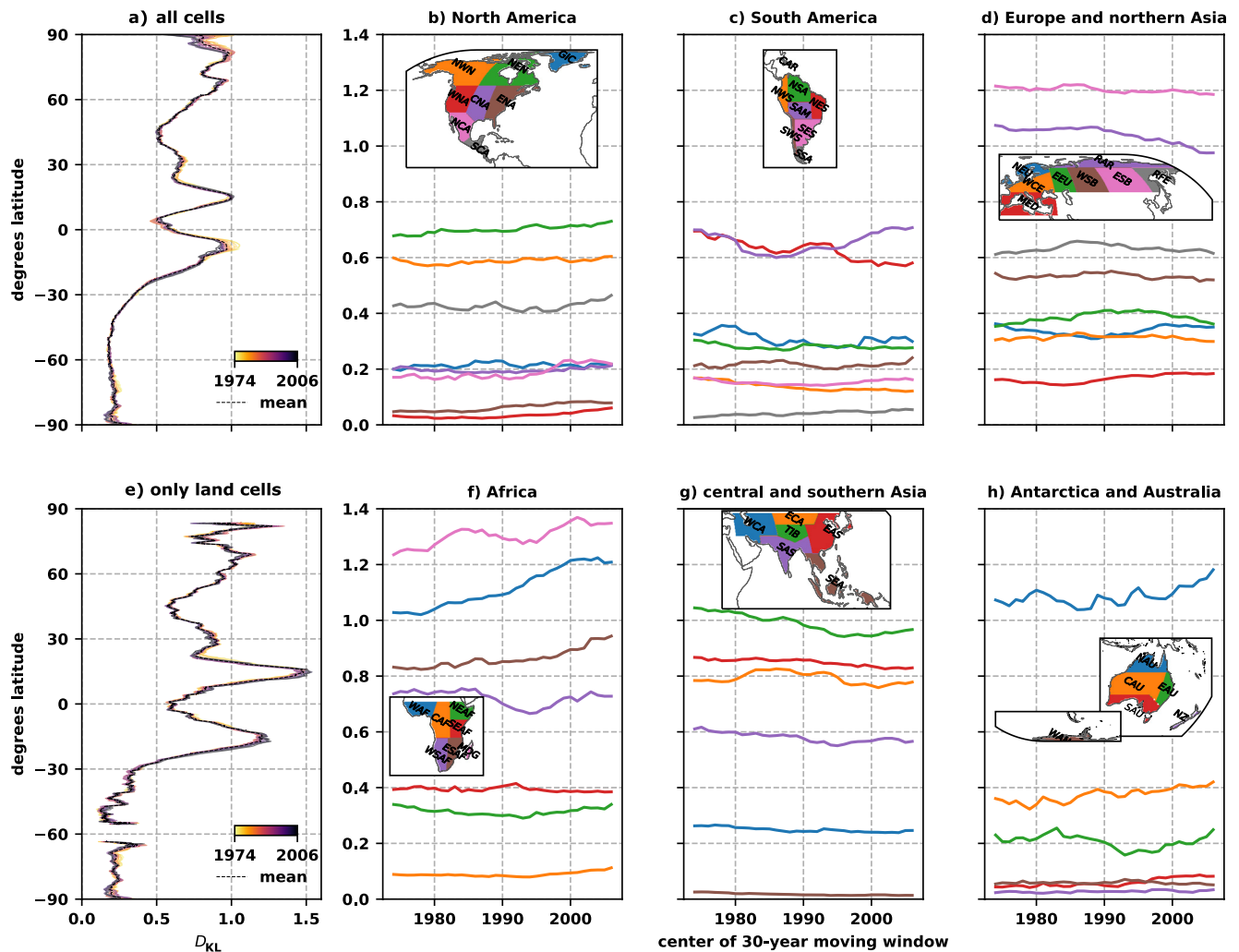
When comparing the relative entropy of extreme precipitation occurrences in ERA5 (Figure 2a) to that of extreme precipitation of gauge data and a regional climate model in the US (Moustakis et al., 2021, their Figures 7a and 7b), the results look largely similar. The main difference is that our threshold of extreme events exhibits a stronger seasonality along the entire west coast and lower seasonality in Arizona and Utah than Moustakis et al. (2021, their Figures 7a and 7b). Furthermore, a comparison of our results to that of monthly precipitation in GPCC (Pascale et al., 2015; Pascale et al., 2016, their Figure 1c), CMAP (Pascale et al., 2015, their Figure 1d), and CMIP5 historical simulations (Pascale et al., 2016, their Figure 1d), similar patterns emerge again. However, the relative entropy of extreme occurrences is higher, indicating a greater clustering of extreme events compared to monthly precipitation. Regions such as northern North America, northern Europe, and various parts of Asia show a particularly pronounced clustering of extremes. Additionally, the geographical features of mountain ranges and coastlines are more prominent in the relative entropy of extreme occurrences compared to monthly precipitation.

Figures 2c and 2d demonstrate the changes in relative entropy between the first and last window for each grid cell and for WGI-v4 reference regions, respectively. The observed changes display a mixed pattern of increases and decreases in precipitation seasonality. Notably, Sub-Saharan Africa, Australia, and North America exhibit increasing trends, suggesting a greater clustering of extreme events. Western Africa and North-Eastern Africa shows the highest increase in D_{KL}, indicating a further intensification of extreme event clustering. Conversely, Asia, the Caribbean and North-East South America display decreasing trends, implying a transition toward a more even distribution of extreme events.

Figures 2e and 2f present the Spearman rank correlation coefficient of D_{KL} over time. The correlation patterns align closely with those seen in ΔD_{KL}, albeit with stronger signals. The correlation coefficient is statistically significant ($p < 0.05$) in 73.0% of all cells and 73.4% of land cells (see Table 1). Out of the significant cells, approximately half of the land cells have become more and less clustered. When correcting for field significance, the results obtained in Figure 2e do not change appreciably (see Figure S3a in Supporting Information S1).

Figures 3a and 3e showcase the zonal means of D_{KL} for each latitude on respectively the global domain and over land only. Lower D_{KL} values are evident in the southern hemisphere, with greater variability observed over land. The subtropics and most northern latitudes exhibit high D_{KL} values. Drier areas display the highest inter-annual spread, encompassing the southernmost and northernmost latitudes, as well as the range between approximately −15 and −5° latitude.

The multidecadal variability in D_{KL} for each WGI-v4 land region are depicted in Figures 3b–3d and 3f–3h. Regions such as the Caribbean, South American Monsoon and Northern Australia display substantial variability, whereas regions such as Western Africa or eastern South Africa show long-term increasing trends. Conversely, regions such as East North America, Southern South America, the Mediterranean, and New Zealand exhibit consistent relative entropy patterns over the years analyzed. Moreover, the highest values of D_{KL}, so the highest

Figure 3. The relative entropy D_{KL} indicating seasonality of extreme daily precipitation occurrences (Equation 1) presented as: (a) mean value for each latitude across grid cells and (e) across land cells. The colorbar in the legend of these panels indicate the middle of a 30-year window. The mean value across all 30-year windows is presented by the dashed black line. Panels (b–d and f–h) show D_{KL} calculated for each WGI-V4 land region. Each line corresponds to a region with the same color as shown on the map in that panel. The x-axis presents the middle of a 30-year window. Dry areas, defined as cells with a mean value of the 90th highest rainfall event below 5 mm day^{-1} in all 30-year windows, are removed from this analysis.

clustering of precipitation extremes, are observed in geographically diverse regions, specifically Western Africa, Madagascar, Tibetan Plateau, Eastern Siberia, Russian Arctic, and Northern Australia.

The mean seasonal centroid C, which represents the timing of extreme precipitation occurrences, is presented in Figure 4. Panel a displays the mean of all 30-year windows for each grid cell, while panel b shows C per WGI-v4 reference region over land. The centroid of extreme precipitation occurrences over extra-tropical land regions predominantly falls in the summer months, with December-February in the Southern Hemisphere and June-August in the Northern hemisphere. The exception is the Mediterranean and west central Asia, where C occurs in winter (January - February). These patterns are comparable to those observed in the GPCC data set over land (Pascale et al., 2015; Pascale et al., 2016, respectively their Figures 15a and 1g), and CMIP5 historical simulations (Pascale et al., 2016, their Figure 1h), indicating a similarity between the centroid of extreme precipitation occurrences and all precipitation. Furthermore, our results closely align to those of Dey et al. (2021, their Figures 2a and 2d), who estimated the timing of extreme precipitation over Australia, defined as the maximum consecutive 5-day precipitation, using the circular mean instead of C.

Figures 4c and 4d present the difference in the number of days between the centroids of the first and last window. In most WGI-V4 regions, there is a difference of only a few days between the first and last window,
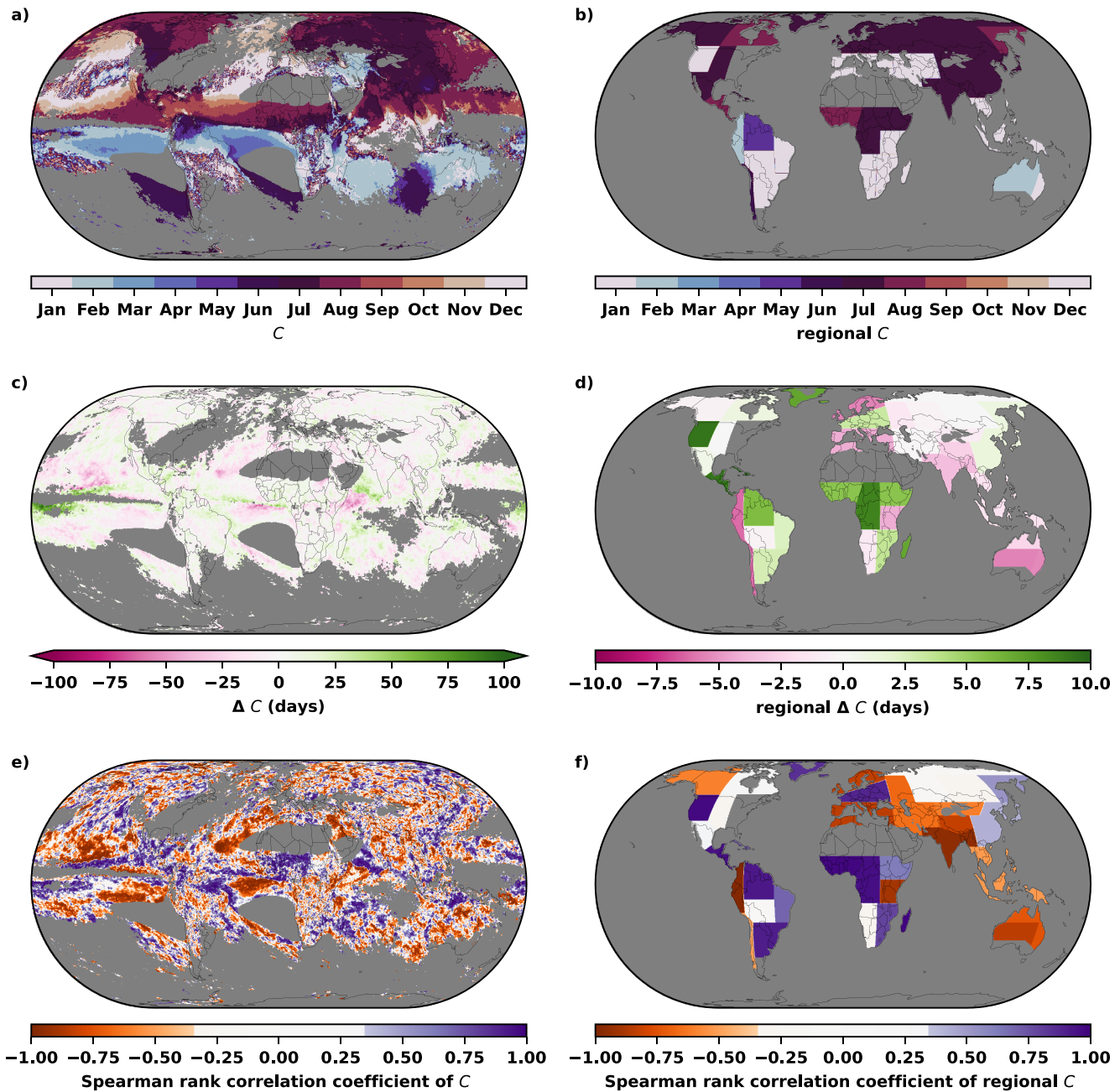
Figure 4. Mean seasonal centroid of the seasonality of extreme daily precipitation occurrences (C, Equation 2). Presented as (a) the mean of all 30-year windows analyzed per grid cell, and (b) calculated per WGI-v4 reference region over land. Panel (c) shows the difference in C between the first and last window for each grid cell in number of days ($\Delta C = C_{1992-2021} - C_{1959-1988}$), with a negative ΔC indicating that the central date of extreme rainfall occurrences are taking place earlier in the year and a positive ΔC indicating later in the year. Panel (d) shows the same difference calculated per WGI-v4 reference region over land. Panel (e) shows the Spearman rank correlation coefficient of C for each grid cell, the non-white values indicate statistical significance ($p < 0.05$). Panel (f) shoes the correlation coefficients calculated per WGI-v4 reference region over land. Cells with $D_{KL} < 0.27$ (rainfall occurrences occurring in more than 10 months) are excluded. Also dry areas, defined as cells with a mean value of the 90th highest rainfall event in all 30-year windows below 5 mm day^{-1}, are masked in gray. Regions in panels (b), (d), and (f) only include those containing at least 50% of the cells based on the two criteria above.

indicating minimal changes in the timing of extreme precipitation occurrences. In some specific regions, such as Australia, western South America, northeastern Europe, the Mediterranean and South Asia, the centroid falls a few days earlier in the year. Conversely in Western North America, South Central America, the Caribbean, eastern South America, and most regions in Sub-Sahran Africa, the centroid occurs a few days later in

the year in the last window compared to the first. The pattern for West Africa is in agreement with findings by Van de Giesen et al. (2010), who noted that the onset of the rainy season has shifted to 10 days later in the year.

Figures 4e and 4f present the Spearman rank correlation coefficient of C over time. Like with Figures 2e and 2f, the correlation patterns are similar with those seen in ΔC. Figure S3b in Supporting Information S1 shows Figure 4e correcting for field significance, displaying very similar patterns. The regional Spearman rank correlation coefficient is significant in 30 of the 38 included regions, half of them have a positive and negative correlation coefficient.

When comparing the significant trends of the relative entropy (D_{KL}, Figure 2f) and seasonal centroid (C, Figure 4f) interesting global patterns emerge. In Australia, the Mediterranean and northwest North America, the value of D_{KL} increases while C decreases. This means a higher degree of clustering combined with extremes that occur earlier. In southern Asia, northwest South America and southeastern Africa, the value of D_{KL} decreases while C decreases too, so more evenly spread out extremes and earlier in the year. In western Africa, central Africa, eastern Southern Africa and Madagascar, both D_{KL} and C are increasing. The same is observed over western North America and Greenland.

4. Conclusions

In this study, we examined the seasonality of extreme daily precipitation occurrences using a metric based on relative entropy (D_{KL}) as an indicator of intra-annual clustering. By analyzing more than 60 years of precipitation data from ERA5 (1959–2021), our findings highlight significant historical shifts in the seasonality of extreme precipitation occurrences across different regions. In Africa, characterized by large seasonality at the beginning of the analyzed time period, we observed a further increase in the concentration of extreme precipitation events during specific times of the year. In Asia, although initial D_{KL} values were also high, a decrease in clustering was observed over time. Australia and North America, characterized by initially low D_{KL} values, experienced an increase in the clustering of extreme precipitation events. In parts of South America D_{KL} has decreased, whereas in Europe D_{KL} has remained relatively constant. Future work may seek to extend this analysis and that of Pascale et al. (2015, 2016) by evaluating whether historical climate model simulations capture the trends in extreme rainfall seasonality we observed in ERA5 reanalysis. Such an approach could then be used for improved projections of future changes in extreme precipitation seasonality.

Examining the timing of extreme precipitation occurrences, we found that the peak of extreme events over extra-tropical land regions typically falls within summer. The observed patterns align with those of monthly precipitation, suggesting a similarity in the seasonality between extreme event occurrence and total precipitation amounts. The observed shift in timing of the centroid usually just spans a few days, suggesting a modest change in the timing of the extreme precipitation events. Changes in the timing of precipitation extremes have implications for flood risk (Blöschl et al., 2017; Wasko et al., 2020a, 2020b), for instance when earlier extreme precipitation occurrences are combined with earlier snowmelt due to increasing global temperatures (Tarasova et al., 2023). Conversely, when extreme events occur outside of the main rainy season, the probabilities of soil erosion and landslides are higher (Steger et al., 2023). As such our work highlights the importance of taking changes in timing of extremes into account in climate adaptation scenarios.

Data Availability Statement

ERA5 data (Hersbach et al., 2018, 2020) were downloaded from the Copernicus Climate Change Service (C3S) (2023) Climate Data Store, using era5cli version 1.3.2 (van Haren et al., 2022). CDO version 1.9.3 was used to pre-process ERA5 data to go from hourly time steps to daily time steps. Data were analyzed using netCDF4 version 1.5.5 (Whitaker et al., 2020), numpy version 1.21.1 (Harris et al., 2020), pandas version 1.3.3 (Reback et al., 2021; Wes McKinney, 2010), regionmask version 0.8.0 (Hauser et al., 2021), scipy version 1.7.1 (Gommers et al., 2021; Virtanen et al., 2020) and xarray version 0.19.0 (Hoyer et al., 2021; Hoyer & Hamman, 2017). Figures were made with cartopy version 0.20 (Met Office, 2010 - 2015; Elson et al., 2022) and Matplotlib version 3.4.3 (Hunter, 2007). The python scripts and NetCDF data for repeating our analyses and recreating the figures and table in this manuscript are stored on the 4TU Repository (Gründemann et al., 2023b).

References

Alexander, L. V. (2016). Global observed long-term changes in temperature and precipitation extremes: A review of progress and limitations in IPCC assessments and beyond. *Weather and Climate Extremes*, *11*, 4–16. https://doi.org/10.1016/j.wace.2015.10.007

Allen, M. R., & Ingram, W. J. (2002). Constraints on future changes in climate and the hydrologic cycle. *Nature*, *419*(6903), 224–232. https://doi.org/10.1038/nature01092

Asadieh, B., & Krakauer, N. Y. (2015). Global trends in extreme precipitation: Climate models versus observations. *Hydrology and Earth System Sciences*, *19*(2), 877–891. https://doi.org/10.5194/hess-19-877-2015

Bal, P. K., Pathak, R., Mishra, S. K., & Sahany, S. (2019). Effects of global warming and solar geoengineering on precipitation seasonality. *Environmental Research Letters*, *14*(3), 034011. https://doi.org/10.1088/1748-9326/aafc7d

Bandhauer, M., Isotta, F., Lakatos, M., Lussana, C., Båserud, L., Izsák, B., et al. (2022). Evaluation of daily precipitation analyses in E-OBS (v19.0e) and ERA5 by comparison to regional high-resolution datasets in European regions. *International Journal of Climatology*, *42*(2), 727–747. https://doi.org/10.1002/joc.7269

Berghuijs, W. R., Harrigan, S., Molnar, P., Slater, L. J., & Kirchner, J. W. (2019). The relative importance of different flood-generating mechanisms across Europe. *Water Resources Research*, *55*(6), 4582–4593. https://doi.org/10.1029/2019WR024841

Blöschl, G., Hall, J., Parajka, J., Perdigão, R. A. P., Merz, B., Arheimer, B., et al. (2017). Changing climate shifts timing of European floods. *Science*, *357*(6351), 588–590. https://doi.org/10.1126/science.aan2506

Chen, H.-P., & Sun, J.-Q. (2013). How large precipitation changes over global monsoon regions by CMIP5 models? *Atmospheric and Oceanic Science Letters*, *6*(5), 306–311. https://doi.org/10.3878/j.issn.1674-2834.13.0002

Copernicus Climate Change Service (C3S). (2023). ERA5 hourly data on single levels from 1959 to present. *Copernicus Climate Change Service (C3S) Climate Data Store (CDS)*. https://doi.org/10.24381/cds.adbb2d47

Cover, T. M., & Thomas, J. A. (2005). Entropy, relative entropy, and mutual information. In *Elements of information theory* (2nd ed., pp. 13–55). John Wiley & Sons, Ltd. https://doi.org/10.1002/047174882X.ch2

Dey, R., Bador, M., Alexander, L. V., & Lewis, S. C. (2021). The drivers of extreme rainfall event timing in Australia. *International Journal of Climatology*, *41*(15), 6654–6673. https://doi.org/10.1002/joc.7218

Donat, M. G., Lowry, A. L., Alexander, L. V., Gorman, P. A. O., & Maher, N. (2016). More extreme precipitation in the world's dry and wet regions. *Nature Climate Change*, *6*(5), 508–513. https://doi.org/10.1038/NCLIMATE2941

Easterling, D. R., Kunkel, K. E., Wehner, M. F., & Sun, L. (2016). Detection and attribution of climate extremes in the observed record. *Weather and Climate Extremes*, *11*, 17–27. https://doi.org/10.1016/j.wace.2016.01.001

Elson, P., de Andrade, E. S., Lucas, G., May, R., Hattersley, R., Campbell, E., et al. (2022). Scitools/cartopy: v0.20.3 [Software]. Zenodo. https://doi.org/10.5281/zenodo.6775197

Feng, X., Porporato, A., & Rodriguez-Iturbe, I. (2013). Changes in rainfall seasonality in the tropics. *Nature Climate Change*, *3*(9), 811–815. https://doi.org/10.1038/NCLIMATE1907

Fernandes, L. G., & Rodrigues, R. R. (2018). Changes in the patterns of extreme rainfall events in southern Brazil. *International Journal of Climatology*, *38*(3), 1337–1352. https://doi.org/10.1002/joc.5248

Fowler, H. J., Lenderink, G., Prein, A. F., Westra, S., Allan, R. P., Ban, N., et al. (2021). Anthropogenic intensification of short-duration rainfall extremes. *Nature Reviews Earth & Environment*, *2*(2), 107–122. https://doi.org/10.1038/s43017-020-00128-6

Gershunov, A., Shulgina, T., Ralph, F. M., Lavers, D. A., & Rutz, J. J. (2017). Assessing the climate-scale variability of atmospheric rivers affecting western North America. *Geophysical Research Letters*, *44*(15), 7900–7908. https://doi.org/10.1002/2017GL074175

Gommers, R., Virtanen, P., Burovski, E., Oliphant, T. E., Weckesser, W., Cournapeau, D., et al. (2021). scipy/scipy: Scipy 1.7.1 [Software]. Zenodo. https://doi.org/10.5281/zenodo.5152559

Greven, A., Keller, G., & Warnecke, G. (2014). *Entropy*. Princeton University Press.

Gründemann, G. J., van de Giesen, N., Brunner, L., & van der Ent, R. (2022). Rarest rainfall events will see the greatest relative increase in magnitude under future climate change. *Communications Earth & Environment*, *3*(235), 235. https://doi.org/10.1038/s43247-022-00558-8

Gründemann, G. J., Zorzetto, E., Beck, H. E., Schleiss, M., van de Giesen, N., Marani, M., & van der Ent, R. J. (2023a). Extreme precipitation return levels for multiple durations on a global scale. *Journal of Hydrology*, *621*, 129558. https://doi.org/10.1016/j.jhydrol.2023.129558

Gründemann, G. J., Zorzetto, E., van de Giesen, N., & van der Ent, R. (2023b). Scripts and data for "historical shifts in seasonality and timing of extreme precipitation" [Dataset, Software]. 4TU Research Data. https://doi.org/10.4121/bac024f1-6c2e-4a09-bf0f-be78b6bbe21c

Harris, C. R., Millman, K. J., van der Walt, S. J., Gommers, R., Virtanen, P., Cournapeau, D., et al. (2020). Array programming with NumPy. *Nature*, *585*(7825), 357–362. https://doi.org/10.1038/s41586-020-2649-2

Hauser, M., Spring, A., Busecke, J., & van Driel, M. (2021). regionmask/regionmask: Version 0.8.0 [Software]. Zenodo. https://doi.org/10.5281/zenodo.5532848

Haylock, M. R., Peterson, T. C., Alves, L. M., Ambrizzi, T., Anunciação, Y. M. T., Baez, J., et al. (2006). Trends in total and extreme South American rainfall in 1960–2000 and links with sea surface temperature. *Journal of Climate*, *19*(8), 1490–1512. https://doi.org/10.1175/JCLI3695.1

Hénin, R., Liberato, M. L. R., Ramos, A. M., & Gouveia, C. M. (2018). Assessing the use of satellite-based estimates and high-resolution precipitation datasets for the study of extreme precipitation events over the Iberian Peninsula. *Water*, *10*(11), 1688. https://doi.org/10.3390/w10111688

Hersbach, H., Bell, B., Berrisford, P., Biavati, G., Horányi, A., Muñoz Sabater, J., et al. (2018). ERA5 hourly data on single levels from 1959 to present [Dataset]. Copernicus Climate Change Service (C3S) Climate Data Store (CDS). https://doi.org/10.24381/cds.adbb2d47

Hersbach, H., Bell, B., Berrisford, P., Hirahara, S., Horanyi, A., Munoz-Sabater, J., et al., (2020). The ERA5 global reanalysis. *Quarterly Journal of the Royal Meteorological Society*, *146*(730), 1–51. https://doi.org/10.1002/qj.3803

Hoyer, S., & Hamman, J. (2017). xarray: N-D labeled arrays and datasets in Python. *Journal of Open Research Software*, *5*(1), 10. https://doi.org/10.5334/jors.148

Hoyer, S., Roos, M., Hamman, J., KeewisCherian, D., Fitzgerald, C., et al. (2021). pydata/xarray: v0.19.0 [Software]. Zenodo. https://doi.org/10.5281/zenodo.5130718

Hunter, J. D. (2007). Matplotlib: A 2d graphics environment. *Computing in Science & Engineering*, *9*(3), 90–95. https://doi.org/10.1109/MCSE.2007.55

IPCC. (2012). Managing the risks of extreme events and disasters to advance climate change adaptation. In *A special report of working groups I and II of the intergovernmental panel on climate change (Tech. Rep.)* (p. 582). Cambridge University Press.

Iturbide, M., Gutiérrez, J. M., Alves, L. M., Bedia, J., Cerezo-Mota, R., Cimadevilla, E., et al., (2020). An update of IPCC climate reference regions for subcontinental analysis of climate model data: Definition and aggregated datasets. *Earth System Science Data*, *12*(4), 2959–2970. https://doi.org/10.5194/essd-12-2959-2020

Kitoh, A., Endo, H., Krishna Kumar, K., Cavalcanti, I. F. A., Goswami, P., & Zhou, T. (2013). Monsoons in a changing world: A regional perspective in a global context. *Journal of Geophysical Research: Atmospheres*, *118*(8), 3053–3065. https://doi.org/10.1002/jgrd.50258

Kullback, S., & Leibler, R. A. (1951). On information and sufficiency. *The Annals of Mathematical Statistics*, *22*(1), 79–86. https://doi.org/10.1214/aoms/1177729694

Kundzewicz, Z. W., Pińskwar, I., & Brakenridge, G. R. (2018). Changes in river flood hazard in Europe: A review. *Hydrology Research*, *49*(2), 294–302. https://doi.org/10.1080/02626667.2016.1241398

Landrum, L., & Holland, M. M. (2020). Extremes become routine in an emerging new arctic. *Nature Climate Change*, *10*(12), 1108–1115. https://doi.org/10.1038/s41558-020-0892-z

Lavers, D. A., Simmons, A., Vamborg, F., & Rodwell, M. J. (2022). An evaluation of era5 precipitation for climate monitoring. *Quarterly Journal of the Royal Meteorological Society*, *148*(748), 3152–3165. https://doi.org/10.1002/qj.4351

Lei, X., Xu, W., Chen, S., Yu, T., Hu, Z., Zhang, M., et al. (2022). How well does the ERA5 reanalysis capture the extreme climate events over China? Part I: Extreme precipitation. *Frontiers in Environmental Science*, *10*. https://doi.org/10.3389/fenvs.2022.921658

Limsakul, A. (2020). Change in rainfall seasonality in Thailand during 1955-2018. *Agriculture and Natural Resources*, *54*(4), 369–376. https://doi.org/10.34044/j.anres.2020.54.4.05

Loeb, N. A., Crawford, A., Stroeve, J. C., & Hanesiak, J. (2022). Extreme precipitation in the eastern Canadian Arctic and Greenland: An evaluation of atmospheric reanalyses. *Frontiers in Environmental Science*, *10*. https://doi.org/10.3389/fenvs.2022.866929

Marc, O., Stumpf, A., Malet, J.-P., Gosset, M., Uchida, T., & Chiang, S.-H. (2018). Initial insights from a global database of rainfall-induced landslide inventories: The weak influence of slope and strong influence of total storm rainfall. *Earth Surface Dynamics*, *6*(4), 903–922. https://doi.org/10.5194/esurf-6-903-2018

Meredith, E. P., Ulbrich, U., & Rust, H. W. (2019). The diurnal nature of future extreme precipitation intensification. *Geophysical Research Letters*, *46*(13), 7680–7689. https://doi.org/10.1029/2019GL082385

Met Office. (20102015). Cartopy: A cartographic python library with a matplotlib interface [computer software manual]. Exeter, Devon. Retrieved from https://scitools.org.uk/cartopy

Miniussi, A., Villarini, G., & Marani, M. (2020). Analyses through the metastatistical extreme value distribution identify contributions of tropical cyclones to rainfall extremes in the eastern United States. *Geophysical Research Letters*, *47*(7), e2020GL087238. https://doi.org/10.1029/2020GL087238

Moustakis, Y., Papalexiou, S. M., Onof, C. J., & Paschalis, A. (2021). Seasonality, intensity, and duration of rainfall extremes change in a warmer climate. *Earth's Future*, *9*(3), 1–15. https://doi.org/10.1029/2020EF001824

Nikolopoulos, E. I., Borga, M., Marra, F., Crema, S., & Marchi, L. (2015). Debris flows in the eastern Italian Alps: Seasonality and atmospheric circulation patterns. *Natural Hazards and Earth System Sciences*, *15*(3), 647–656. https://doi.org/10.5194/nhess-15-647-2015

Papalexiou, S. M., & Montanari, A. (2019). Global and regional increase of precipitation extremes under global warming. *Water Resources Research*, *55*(6), 4901–4914. https://doi.org/10.1029/2018WR024067

Pascale, S., Lucarini, V., Feng, X., Porporato, A., & Hasson, S. (2015). Analysis of rainfall seasonality from observations and climate models. *Climate Dynamics*, *44*(11–12), 3281–3301. https://doi.org/10.1007/s00382-014-2278-2

Pascale, S., Lucarini, V., Feng, X., Porporato, A., & Hasson, S. (2016). Projected changes of rainfall seasonality and dry spells in a high greenhouse gas emissions scenario. *Climate Dynamics*, *46*(3–4), 1331–1350. https://doi.org/10.1007/s00382-015-2648-4

Pendergrass, A. G., & Knutti, R. (2018). The uneven nature of daily precipitation and its change. *Geophysical Research Letters*, *45*(11), 980–988. https://doi.org/10.1029/2018GL080298

Pfahl, S., Gorman, P. A. O., & Fischer, E. M. (2017). Understanding the regional pattern of projected future changes in extreme precipitation. *Nature Climate Change*, *7*(6), 423–428. https://doi.org/10.1038/NCLIMATE3287

Reback, J., jbrockmendel, McKinney, W., Van den Bossche, J., Augspurger, T., Cloud, P., et al. (2021). pandas-dev/pandas: Pandas 1.3.3 [Software]. Zenodo. https://doi.org/10.5281/zenodo.5501881

Sahany, S., Mishra, S. K., Pathak, R., & Rajagopalan, B. (2018). Spatiotemporal variability of seasonality of rainfall over India. *Geophysical Research Letters*, *45*(14), 7140–7147. https://doi.org/10.1029/2018GL077932

Shen, L., Wen, J., Zhang, Y., Ullah, S., Meng, X., & Chen, G. (2022). Performance evaluation of ERA5 extreme precipitation in the Yangtze river delta, China. *Atmosphere*, *13*(9), 1416. https://doi.org/10.3390/atmos13091416

Steger, S., Moreno, M., Crespi, A., Zellner, P. J., Gariano, S. L., Brunetti, M. T., et al. (2023). Deciphering seasonal effects of triggering and preparatory precipitation for improved shallow landslide prediction using generalized additive mixed models. *Natural Hazards and Earth System Sciences*, *23*(4), 1483–1506. https://doi.org/10.5194/nhess-23-1483-2023

Tandon, N. F., Zhang, X., & Sobel, A. H. (2018). Understanding the dynamics of future changes in extreme precipitation intensity. *Geophysical Research Letters*, *45*(6), 2870–2878. https://doi.org/10.1002/2017GL076361

Tarasova, L., Lun, D., Merz, R., Blöschl, G., Basso, S., Bertola, M., et al. (2023). Shifts in flood generation processes exacerbate regional flood anomalies in Europe. *Communications Earth & Environment*, *4*(1), 49. https://doi.org/10.1038/s43247-023-00714-8

Tramblay, Y., Arnaud, P., Artigue, G., Lang, M., Paquet, E., Neppel, L., & Sauquet, E. (2023). Changes in mediterranean flood processes and seasonality. *Hydrology and Earth System Sciences*, *27*(15), 2973–2987. https://doi.org/10.5194/hess-27-2973-2023

Van de Giesen, N., Liebe, J., & Jung, G. (2010). Adapting to climate change in the Volta Basin, West Africa. *Current science*, *98*(8), 1033–1037.

van Haren, R., Camphuijsen, J., Dzigan, Y., Drost, N., Alidoost, F., Andela, B., et al. (2022). era5cli [Software]. Zenodo. https://doi.org/10.5281/zenodo.7433273

Virtanen, P., Gommers, R., Oliphant, T. E., Haberland, M., Reddy, T., Cournapeau, D., et al., (2020). SciPy 1.0: Fundamental algorithms for scientific computing in python. *Nature Methods*, *17*(3), 261–272. https://doi.org/10.1038/s41592-019-0686-2

Wang, P., Huang, Q., Tang, Q., Chen, X., Yu, J., Pozdniakov, S. P., & Wang, T. (2021). Increasing annual and extreme precipitation in permafrost-dominated Siberia during 1959–2018. *Journal of Hydrology*, *603*, 126865. https://doi.org/10.1016/j.jhydrol.2021.126865

Wasko, C., Nathan, R., & Peel, M. C. (2020a). Changes in antecedent soil moisture modulate flood seasonality in a changing climate. *Water Resources Research*, *56*(3). https://doi.org/10.1029/2019WR026300

Wasko, C., Nathan, R., & Peel, M. C. (2020b). Trends in global flood and streamflow timing based on local water year. *Water Resources Research*, *56*(8). https://doi.org/10.1029/2020WR027233

Wes McKinney (2010). Data structures for statistical computing in Python. In S. van der Walt & J. Millman (Eds.), *Proceedings of the 9th Python in science conference* (pp. 56–61). https://doi.org/10.25080/Majora-92bf1922-00a

Westra, S., Fowler, H. J., Evans, J. P., Alexander, L. V., Berg, P., Johnson, F., et al. (2014). Future changes to the intensity and frequency of short-duration extreme rainfall. *Reviews of Geophysics*, *52*(3), 522–555. https://doi.org/10.1002/2014RG000465

Whitaker, J., Khrulev, C., Huard, D., Paulik, C., Hoyer, S., Filipe, et al. (2020). Unidata/netcdf4-python: Version 1.5.5 release [Software]. Zenodo. https://doi.org/10.5281/zenodo.4308773

Wilks, D. S. (2016). "The stippling shows statistically significant grid points": How research results are routinely overstated and overinterpreted, and what to do about it. *Bulletin of the American Meteorological Society*, *97*(12), 2263–2273. https://doi.org/10.1175/BAMS-D-15-00267.1